

Direct Measurement of Sub-Debye-Length Attraction between Oppositely Charged Surfaces

Nir Kampf,¹ Dan Ben-Yaakov,² David Andelman,² S. A. Safran,¹ and Jacob Klein^{1,*}

¹*Department of Materials and Interfaces, Weizmann Institute of Science, Rehovot 76100, Israel*

²*Raymond and Beverly Sackler School of Physics and Astronomy, Tel Aviv University, Ramat Aviv, Tel Aviv 69978, Israel*

(Received 15 May 2009; published 11 September 2009)

Using a surface force balance with fast video analysis, we have measured directly the attractive forces between oppositely charged solid surfaces (charge densities σ_+ , σ_-) across water over the entire range of interaction, in particular, at surface separations D below the Debye screening length λ_S . At very low salt concentration we find a long-ranged attraction between the surfaces (onset ca. 100 nm), whose variation at $D < \lambda_S$ agrees well with predictions based on solving the Poisson-Boltzmann theory, when due account is taken of the independently-determined surface charge asymmetry ($\sigma_+ \neq |\sigma_-|$).

DOI: 10.1103/PhysRevLett.103.118304

PACS numbers: 82.70.-y, 07.10.Pz, 82.45.Mp

The Debye-Hückel, and more generally the Derjaguin-Landau-Verwey-Overbeek approach, based on linearization of the Poisson-Boltzmann (PB) theory, are used classically to calculate the repulsive interactions between uniform symmetrically-charged surfaces, and their predictions have been amply verified [1,2]. In 1972, Parsegian and Gingell [3] extended this to interactions between *unequally*-charged surfaces in the low surface potential limit (as may result from strong electrostatic screening at high salt concentration c_b). In that limit (where the theory may be linearized) the range of the interaction scales with the Debye screening length $\lambda_S = (\epsilon \epsilon_0 k_B T / 2e^2 c_b)^{1/2}$; here ϵ_0 is the permittivity of free space, ϵ is the dielectric constant, k_B the Boltzmann constant, T the absolute temperature, and e the electronic charge. For unequally-charged surfaces the forces may be attractive or repulsive [3], but in the case of surfaces whose charge densities are equal and opposite (i.e., antisymmetric), $\sigma_+ = |\sigma_-|$, the forces are monotonically attractive as a function of D . For $D > \lambda_S$, such attraction is predicted to decay exponentially with D [3]. Qualitatively, this attraction may be viewed [4] as due to the entropy gain arising through release of counterion pairs from the intersurface gap into the surrounding reservoir, as the surfaces approach. Direct measurements [5–9] of forces between approaching, oppositely charged surfaces in the Parsegian-Gingell regime reveal the onset of measurable attraction at $D \approx (1.5\text{--}3)\lambda_S$, followed by jumps into contact from these separations due to mechanical instability of the measuring devices [10]; the magnitude of the attraction during the jumps could not be measured. Recently the case of oppositely charged surfaces across water at very low bulk salt concentration c_b was treated theoretically [4,11,12], where the high surface potential ψ necessitates solution of the PB equation:

$$\nabla^2 \psi = (2ec_b / \epsilon \epsilon_0) \sinh(e\psi / k_B T). \quad (1)$$

This low-salt regime is of special interest because the attraction between the surfaces can be significant over a surface separation range of order 50 nm or more, which is

nonetheless smaller than the screening length λ_S (recalling $\lambda_S \propto c_b^{-1/2}$). In this regime the attraction predicted by the nonlinear theory [Eq. (1)] scales approximately as $(1/D^2)$ [4]. Here we measure directly the forces between two oppositely charged surfaces as a function of their separation across water with no added salt. Our results reveal a long-ranged attraction, which at its onset (at $D =$ ca. 100 nm) is many orders of magnitude larger than van der Waals (vdW) attraction. Using fast video recording we are able to characterize the attraction between the surfaces continuously as they come into contact. We find that the measured forces agree well with the variation given by the PB theory [Eq. (1)] [12–14] at all surface separations D , particularly at $D < \lambda_S$ where its predictions diverge from those of the linearized treatment [3], when proper account is taken of the (independently-determined) asymmetry in the surface charge density.

We use a surface force balance (SFB) [15] (see schematic inset to Fig. 1), with high sensitivity in measuring both normal forces, $F_n(D)$, and especially shear forces, $F_s(D)$, between two molecularly smooth, curved mica surfaces (curvature radius $R \approx 1$ cm) as a function of their absolute separation D . The high sensitivity, necessary for detailed examination of the forces, requires a weak force-measuring spring K_n , which in turn leads to a spontaneous jump-in of the surfaces [10] as in previous studies [7,9]. We measure forces during the jump-in via a *dynamic* measurement, using fast video recording of the SFB optical interference fringes which, with frame grabbing and solution of the optical equations, reveals the variation with time t of the separation $D(t)$ of the surfaces. From $D(t)$ the resulting normal force $F_n(D)$ between the surfaces is evaluated from the instantaneous balance of forces [16], using Eq. (2) below:

$$F_n(D) = m \left(\frac{d^2 D}{dt^2} \right) - K_n (\delta D(t)) + 6\pi R^2 \eta \left[\left(\frac{dD}{dt} \right) / D(t) \right], \quad (2)$$

where m is the total mass of the (moving) lower surface, K_n

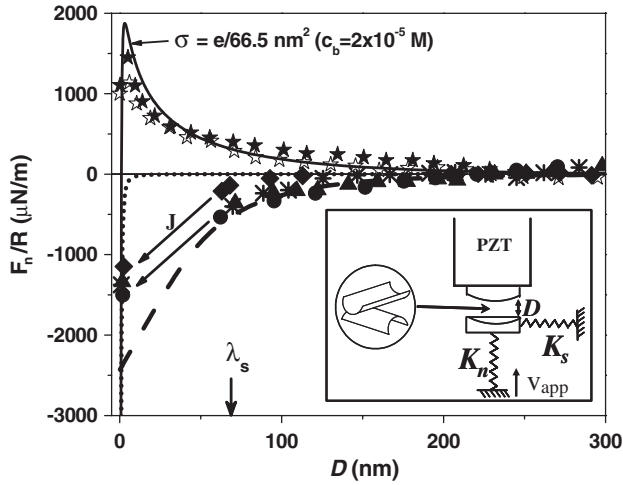


FIG. 1. Normal force profiles $F_n(D)/R$ between curved mica surfaces (mean radius R) across water with no added salt. \star , \triangle : interactions between bare mica surfaces (from independent experiments, i.e., different pairs of mica sheets). The solid curve is the prediction based on the PB equation [Eq. (1)] with constant surface charge density $\sigma_- = e/(66.5 \text{ nm}^2)$, a 1:1 electrolyte concentration $c_b = 2 \times 10^{-5} \text{ M}$ (derived from the Debye screening length at $D \gg \lambda_D$) and a vdW attraction $F_{\text{vdW}}(D)/R = -A/6D^2$, with $A = 2 \times 10^{-20} \text{ J}$. Solid black symbols (from different experiments and contact points): interactions between a chitosan-coated and a bare mica surface; the arrows indicate the jump-in (J) at the point of mechanical instability, expected for $(\partial F_n/\partial D) \geq K_n$. Broken curve: predicted interaction [4,12] based on antisymmetric surface charge densities, $\sigma_+ = |\sigma_-| = e/(66.5 \text{ nm}^2)$. Dotted curve: vdW attraction $F_{\text{vdW}}(D)/R = -A/6D^2$, with $A = 2 \times 10^{-20} \text{ J}$. (asterisks and diamonds: 2nd approach of surfaces at 2 different contact points in different experiments; circles and triangles: 1st and 6th approaches, respectively, at a given contact point in a different experiment). The inset shows the schematic of the SFB with the two surfaces facing each other in a crossed-cylinder configuration; K_n and K_s are the constants of the normal and shear springs, respectively, PZT is the sectorized piezocrystal, and v_{app} the applied velocity of the normal spring mount (bottom) in the dynamic mode [see Eq. (2)].

is the normal spring constant (150 N/m), and η is the viscosity of the liquid in the gap ($\eta = \eta_{\text{water}} = 0.85 \times 10^{-3} \text{ Pa}\cdot\text{s}$). $\delta D(t)$ is the deflection of the spring, given by $\delta D(t) = D_{t=0} - D(t) + v_{\text{app}}t$, where v_{app} is the inward applied velocity (in the range 10–20 nm/sec, see also inset to Fig. 1), and is determined from the video recording at large separations where $F_n(D) \approx 0$. The first and second terms on the right-hand side of Eq. (2) are the inertial and spring-bending contributions to the force, while the third is the Reynolds-Taylor hydrodynamic lubrication force between the moving surfaces [17].

Force profiles between mica surfaces in pure water (Milli-Q Gradient A10 purification system, water resistivity $18.2 \text{ M}\Omega$ and total organic content $\leq 3\text{--}4 \text{ ppb}$) were measured as previously detailed [16]. Mica loses surface

K^+ ions in water to become negatively-charged, with consequent repulsive forces $F_n(D)$ between two similar surfaces (the K^+ ions disperse throughout the volume and contribute negligibly to the effective salt concentration). The effective salt concentration is evaluated via the far-field decay length λ_D of the forces, while the effective charge density σ_- on each bare mica surface may be extracted via a fit to the $F_n(D)$ profiles based on the PB equation (1) with the condition of constant surface charge. Following this, one surface was then removed and coated with chitosan [18], a positively-charged polysaccharide. The chitosan adsorbs from aqueous solution (followed by washing to remove excess), as previously described [18], to form a thin layer which reverses the charge on the mica, through charge overcompensation, from net negatively charged to net positively charged, as seen at once from the resulting forces. Atomic force microscopy (not shown) was used to characterize the chitosan layer topography, revealing a uniformly coated surface smooth to $2 \pm 0.4 \text{ nm}$ rms over a $1 \times 1 \mu\text{m}^2$ area.

Figure 1 shows normalized force profiles $F_n(D)/R$ between the bare mica surfaces measured across pure water in the usual quasistatic way, i.e., via monitoring of the spring bending during stepwise changes in D [15]. A long-ranged repulsion due to counterion osmotic pressure is observed (star symbols), with measurable forces setting on from $D = \text{ca. } 200 \text{ nm}$, with a Debye length $\lambda_D = 68 \pm 8 \text{ nm}$ evaluated from the far-field regime ($D > \lambda_D$). This value corresponds to an effective salt concentration of $(2 \pm 0.5) \times 10^{-5} \text{ M}$ 1:1 electrolyte (attributed to dissolved atmospheric CO_2 , the extent of which may be evaluated from the slightly acidic pH of our solutions, $\text{pH} = 5.8 \pm 0.2$, and residual ions leached from the glassware [19]). Using this value for c_b we extract the effective bare mica surface charge density $|\sigma_-| = e/(66.5 \text{ nm}^2)$ through a best fit of the data using the PB equation [Eq. (1)] with constant surface charge (augmented by a vdW attraction term [2] $F_{\text{vdW}}(D)/R = -(A/6D^2)$, with $A = 2 \times 10^{-20} \text{ J}$), shown as the solid curve in the upper part of the figure. As in earlier studies [16] the surfaces jump under vdW attraction from a separation $3 \pm 0.5 \text{ nm}$ into adhesive contact. After coating the upper surface with chitosan to reverse its charge a monotonic attraction, larger than the scatter in the data, sets on at $D \approx 100 \text{ nm}$, with the surfaces jumping [10] from $D = \text{ca. } 60 \text{ nm}$ into an adhesive contact at $D = 2 \pm 0.3 \text{ nm}$ (a measure of the thickness of the compressed chitosan coating). The dashed curve is the predicted attraction based on solving the PB equation, Eq. (1) (for $c_b = 2 \times 10^{-5} \text{ M}$), for antisymmetric surface charge densities, i.e. $\sigma_+ = |\sigma_-| (= e/(66.5 \text{ nm}^2))$, neglecting any vdW contribution. We see that indeed the onset of attraction and its magnitude are reasonably predicted by this approach, and in particular that the jumps-in to contact (arrows in Fig. 1) occur roughly where the slope of the predicted $F_n(D)$ curve equals K_n , as expected [10]. We

emphasize that there is negligible, if any, transfer of chitosan between the bare and coated mica surfaces when they come into contact; this is demonstrated by the fact that 1st, 2nd and 6th approaches (Fig. 1 caption) of the surfaces at given contact points show very similar attractive profiles.

To proceed, we confirm that the onset of the measured long-ranged attraction is not due to large, positively-charged polymer loops extending from the adsorbed chitosan layers, which are known to lead to long-ranged attractive bridging forces [20] (bearing in mind the large radius of gyration of the chitosan, $R_g \approx 100$ nm [18]). To do this we measure the *shear* forces between the bare mica and the chitosan-bearing mica. The resulting shear force traces are shown in Fig. 2, and reveal that there is little shear force between the surfaces as they approach down to the jump-in separation. By clamping the normal force springs, we are also able to suppress the jump-in, and thus to show that shear forces are within the scatter down to $D < \text{ca. } 3$ nm. Since shear forces are very sensitive to any bridging by the polymer chains [21,22], this confirms that loops from the chitosan layer do not extend beyond a few nm from the mica surface, and that the long-ranged attraction is due purely to electrostatic effects.

To obtain the $F_n(D)$ profile over the entire range of the interaction—including, in particular, the jump-into-contact regime—we carried out dynamic measurements using fast video recording and frame-grabbing analysis described

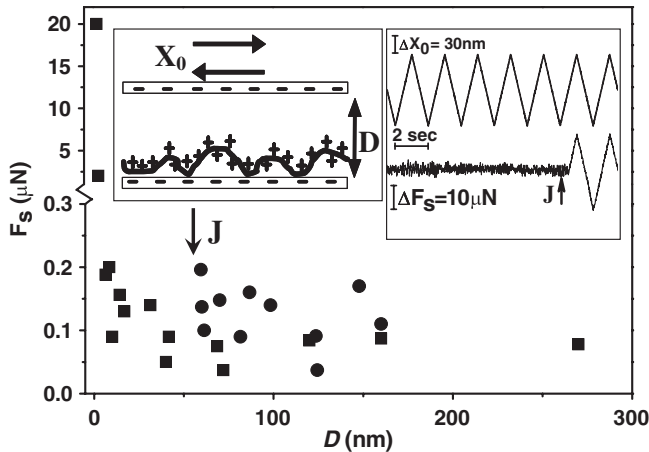


FIG. 2. Shear force $F_s(D)$ profiles between a chitosan-coated surface and a bare mica surface sliding past it at separation D , where X_0 is the applied lateral motion. The cartoon illustrates the adsorption on the lower mica surface of the positively charged chitosan, interacting with the negatively charged upper mica surface. The right inset shows the actual traces, the top one being the back-and-forth sliding motion of the top surface, and the lower trace being the shear force transmitted between the surfaces. When the lower surface is free (filled circles) there is little shear force above the noise until the surfaces jump into contact at J . On clamping the lower surface (squares) to suppress any jump-in, F_s is measurable—revealing little shear force above the noise—right down to $D \approx 3$ nm.

above [Eq. (2)]. The results are shown in Fig. 3. For the symmetric (mica-mica) repulsive regime (large open circles and squares) the dynamic data are within the scatter of the quasistatic force profiles from Fig. 1, and very close to the predicted variation (dashed top curve, taken from Fig. 1). For the case of attracting oppositely charged surfaces, the dynamic profiles all fall within a small range (diamonds and empty circles show profiles at the extremes of the range, with the striped region including 3 other dynamic profiles, not shown for clarity). The five attractive profiles summarized in Fig. 3 include interactions both on a first approach as well as on subsequent approaches: We found no systematic differences between a first approach and second or subsequent approaches at the same contact point, indicating that little if any transfer of the polyelectrolyte was occurring between the surfaces. The range of

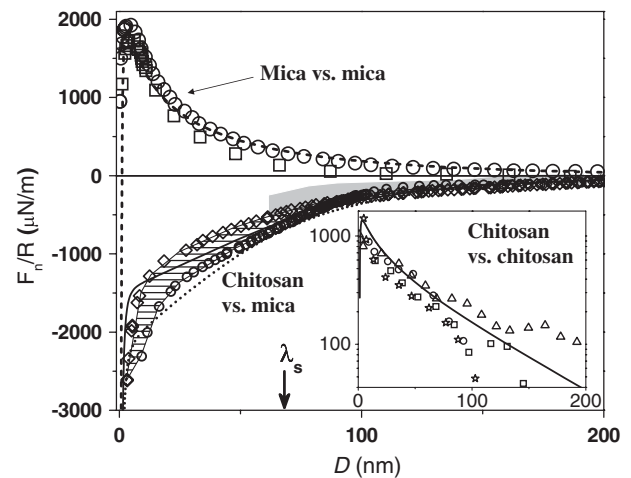


FIG. 3. Normal force profiles $F_n(D)/R$ between two mica surfaces (either bare or coated with chitosan) measured dynamically via fast-rate video recording across water with no added salt. Repulsive profiles between bare mica surfaces are shown by the open circles and squares (from independent experiments, i.e., different pairs of mica sheets), and the dashed curve is the theoretical prediction from Fig. 1. All attractive profiles between a bare and a chitosan-coated mica surface fall in the striped region shown: diamond and empty circles are data for dynamic profiles at the two extremes of this spread, which include 3 additional dynamic profiles (not shown for clarity). The grey band is the range of measured quasistatic profiles from Fig. 1. Dotted curve: predicted forces for antisymmetric case $\sigma_+ = |\sigma_-| = e/(66.5 \text{ nm}^2)$ as in Fig. 1 but augmented by vdW attraction $F_{\text{vdW}}(D)/R = -A/6D^2$, with $A = 2 \times 10^{-20}$ J. Solid curve: predicted forces (based on solution of the PB Eq. (1) with constant charge condition) for the asymmetric case $\sigma_+ = e/(90 \text{ nm}^2)$, $|\sigma_-| = e/(66.5 \text{ nm}^2)$ and $c_b = 2 \times 10^{-5} M$, augmented by $F_{\text{vdW}}(D)/R$ as above. Inset: Quasistatically measured $F_n(D)/R$ profiles between two chitosan-coated mica surfaces (different symbols are for different contact points). The curve is the prediction based on solution of the PB [Eq. (1)] with constant charge condition and $c_b = 2 \times 10^{-5} M$ and $\sigma_+ = e/(90 \text{ nm}^2)$ on both surfaces, augmented by $F_{\text{vdW}}(D)/R$ as above.

dynamic profiles is also similar to the quasistatic data from Fig. 1, indicated as a lightly-shaded region in Fig. 3, where they overlap prior to the jump-in. The dynamic profiles show a rapid increase in attraction at lower D values ($D < \text{ca. } 15 \text{ nm}$), indicating the importance of accounting for vdW attraction. This is implemented in the dotted curve, which represents the antisymmetric prediction $\sigma_+ = |\sigma_-|$ from Fig. 1 augmented by a vdW attraction term $F_{\text{vdW}}(D)/R$ as in Fig. 1. The agreement with the data is then improved, but a discrepancy remains over the range $10 \text{ nm} < D < 60 \text{ nm}$ where the antisymmetric prediction is outside the range of the measured profiles. To account for this we must consider the possibility that the opposing charge densities may be asymmetric, $\sigma_+ \neq |\sigma_-|$. This is done by measuring independently, in a separate (quasistatic) experiment, the normal force profile between two similarly chitosan-coated surfaces across water, inset to Fig. 3. Fitting this profile using the PB equation [Eq. (1)] with constant surface charge, augmented with the same vdW attraction as above, then yields a surface density $\sigma_+ = e/[(90 \pm 10) \text{ nm}^2]$. This independently determined value of σ_+ for the chitosan-coated surface, together with σ_- for the mica taken at its value determined from the bare-mica/bare-mica profiles, and incorporating vdW attraction as above, is then used to calculate the profile shown as the solid curve in Fig. 3. Agreement of the theory with experiment over almost all the range of attraction then becomes much closer. We remark that the crossover from attractive to repulsive electrostatic interaction expected theoretically [3] for the asymmetric case $\sigma_+ \neq |\sigma_-|$ is predicted to occur in the range $D < \text{ca. } 10 \text{ nm}$ already dominated by the vdW attraction, and so is not seen in the calculated curve.

In conclusion, we have measured directly the forces between oppositely charged surfaces across water as a function of their surface separation D , at low salt concentrations where the Debye screening length $\lambda_s \approx 70 \text{ nm}$ comprises a substantial part of the range of measurable attraction (ca. 100 nm). Dynamic surface force balance measurements, using a rapid video recording technique, enabled a detailed examination of the attractive forces, particularly in the regime $D < \lambda_s$, inaccessible to earlier studies. Our results, taking due account of the independently determined charge asymmetry on the interacting surfaces, are in close agreement with predictions [11–14] of the Poisson-Boltzmann theory for interactions in this regime.

We thank the Israel Science Foundation (grants to J. K., to D. A. and to S. A. S.), the Minerva Foundation and the Schmidt Minerva Center for Supramolecular Architecture at the Weizmann Institute (J. K.), and the US-Israel Binational Science Foundation (grants to D. A. and to

S. A. S.) for their support of this work. D. A. thanks the Weizmann Institute. This research was made possible in part by the historic generosity of the Harold Perlman Family.

*Jacob.klein@weizmann.ac.il

- [1] S. A. Safran, *Statistical Thermodynamics Of Surfaces, Interfaces And Membranes* (Addison-Wesley, New York, 1994).
- [2] J. N. Israelachvili, *Intermolecular And Surface Forces* (Academic Press Limited, London, 1992).
- [3] V. A. Parsegian and D. Gingell, *Biophys. J.* **12**, 1192 (1972).
- [4] S. A. Safran, *Europhys. Lett.* **69**, 826 (2005).
- [5] K. Besteman *et al.*, *Phys. Rev. Lett.* **93**, 170802 (2004).
- [6] K. Besteman, M. A. G. Zevenbergen, and S. G. Lemay, *Phys. Rev. E* **72**, 061501 (2005).
- [7] M. Giesbers, J. M. Kleijn, and M. A. Cohen Stuart, *J. Colloid Interface Sci.* **252**, 138 (2002).
- [8] P. G. Hartley and P. J. Scales, *Langmuir* **14**, 6948 (1998).
- [9] K. Lowack and C. A. Helm, *Macromolecules* **31**, 823 (1998).
- [10] Sensitivity in measuring forces $F(D)$ between surfaces D apart requires springs of low constant K_n , leading to Euler-like instabilities and jumps-in whenever $dF/dD > K_n$.
- [11] A. A. Meier-Koll, C. C. Fleck, and H. H. von Grunberg, *J. Phys. Condens. Matter* **16**, 6041 (2004).
- [12] D. Ben-Yaakov *et al.*, *Europhys. Lett.* **79**, 48002 (2007).
- [13] S. H. Behrens and M. Borkovec, *Phys. Rev. E* **60**, 7040 (1999).
- [14] D. McCormack, S. L. Carnie, and D. Y. C. Chan, *J. Colloid Interface Sci.* **169**, 177 (1995).
- [15] J. Klein and E. Kumacheva, *J. Chem. Phys.* **108**, 6996 (1998).
- [16] U. Raviv *et al.*, *Langmuir* **20**, 5322 (2004).
- [17] D. Y. C. Chan and R. G. Horn, *J. Chem. Phys.* **83**, 5311 (1985).
- [18] The chitosan used and the adsorption procedure are identical to that described in N. Kampf, U. Raviv, and J. Klein, *Macromolecules* **37**, 1134 (2004); it has average molecular mass $M = 6 \times 10^5 \text{ Da}$ and 85% degree of deacetylation.
- [19] While the level of residual ions is difficult to control, there is substantial reproducibility between different experiments in water with no added salt (S. Perkin *et al.*, *Langmuir* **22**, 6142 (2006)); this is true particularly for a given set of experiments using mica from the same batch as in the present study, as seen in different force profiles in Figs. 1 and 3.
- [20] J. Klein and P. F. Luckham, *Nature (London)* **308**, 836 (1984).
- [21] E. Eiser *et al.*, *Phys. Rev. Lett.* **82**, 5076 (1999).
- [22] U. Raviv, R. Tadmor, and J. Klein, *J. Phys. Chem. B* **105**, 8125 (2001).